Catalytic H_2 evolution with CoO, $Co(OH)_2$ and CoO(OH) NPs generated from a molecular polynuclear Co complex

Marcos Gil-Sepulcre,[a,b] Carolina Gimbert-Suriñach,[b] David Aguilà,[c] Verónica Velasco,[c] Jordi García-Antón,[a] Antoni Llobet,[a,b] Guillem Aromí,*[c] Roger Bofill*[a] and Xavier Sala*[a]

Abstract: Electrochemical water reduction by employing first row transition metal nanoparticles (NPs) constitutes a sustainable way for the generation of H_2. We have synthesized Co-based NPs from a molecular Co^{II}/Co^{III} precursor after its reductive decomposition at -1.86 V *vs.* NHE in different organic solvents. These NPs are able to electrochemically reduce water at pH 14. SEM, EDX and XPS analyses have allowed the determination of the chemical nature of the as-deposited NPs: CoO when using MeCN as solvent and CoO(OH) when employing either dichloromethane (DCM) or MeOH. After 2h of constant polarization at 10 $mA \cdot cm^{-2}$, the electrocatalytic activity of the NPs obtained in MeCN and DCM decreases, whereas for those obtained in MeOH increases. In this solvent, the overpotential is reduced by 215-220 mV and the specific current density is triplicated. Interestingly, during this activation process in MeOH the precursor CoO(OH) NPs are converted into $Co(OH)_2$. The implications of these results in the context of the current research in the field are also discussed.

Introduction

During the last decade, the struggle against global warming has been centered in attaining sustainable fuel generation systems. The generation of H_2 through the (photo)electrochemical reduction of protons is one of the most promising alternatives.[1] In this context, several transition metal nanoparticles (NPs) have been shown to be catalytically active in the hydrogen evolution reaction (HER),[2] from which cobalt, a relatively abundant 1st row transition metal, constitutes a good cheap candidate.[3]

Co, CoO and $Co(OH)_2$ NPs have been successfully tested as catalysts for the HER at pH 13-14. Further, Co NPs have been encapsulated within carbon shells, carbon nanotubes (CNTs) and carbon nanofibers (CNFs) with a varied range of activities (from -196 to -375 mV overpotentials at 10 $mA \cdot cm^{-2}$ -from now on η-) and good stability (5.5-10 h electrolysis).[3b,3c,4] Also, mixed Co/CoO NPs have been deposited on N-doped graphitic C[5] and Co NPs on N,S-doped C,[6] with decreased η values of -395 and -250 mV, respectively, which remarkably further decreases to -50 mV if the Co NPs are embedded inside a CoO matrix.[7] Finally, $Co(OH)_2$ NPs with variable sizes (from 1 to 30 nm) have also been successfully tested at neutral or slightly basic pH under different supports in photocatalytic hydrogen evolution.[8,9]

In the last few years, the *in-situ* formation of catalytically active metal and metal oxide/hydroxide NPs from the decomposition of molecular precursors under catalytic conditions has been indeed described. This is very common in redox catalysis where ligands and metal centres are exposed to oxidative/reductive stress. In the case related to water oxidation, the work of Spiccia and co-workers dealing with the formation of MnO_x NPs inside a Nafion matrix from a wide set of structurally diverse Mn-based complexes under photoelectrochemical catalytic conditions is particularly revealing.[10] The size and catalytic performance of the formed NPs is found to be highly dependent on the structure of the molecular precursor and thus on the nature of the ligands bonded to the Mn ion. For the particular case of Co ions, the *in-situ* formation of $Co(OH)_x$ and CoO_x NPs as the real active catalytic water oxidation species when starting from mononuclear Co complexes and from a Co polyoxometalate, respectively, has also been described.[11] Interestingly, formation of Co-derived NPs has also been observed under HER catalytic conditions at modest cathodic potentials (-0.75 V *vs.* NHE) in the presence of acid in acetonitrile.[3a]

a Dr. R. Bofill, Dr. X. Sala, M. Gil-Sepulcre, Dr. J. García-Antón, Prof. A. Llobet
Departament de Química, Facultat de Ciències
Universitat Autònoma de Barcelona
08193 Bellaterra, Catalonia (Spain)
E-mail: roger.bofill@uab.cat, xavier.sala@uab.cat
Homepage: https://seloxcat.wordpress.com

b M. Gil-Sepulcre, Dr. C. Gimbert-Suriñach, Prof. A. Llobet
Institut Català d'Investigació Química (ICIQ), Barcelona Institute of Science and Technology (BIST)
Av. Països Catalans 16, 43007 Tarragona, Catalonia (Spain)

c Dr. G. Aromí, Dr, D. Aguilà, Dr. V. Velasco
Departament de Química Inorgànica i Orgànica
Universitat de Barcelona
Avda. Diagonal 645, 08028 Barcelona, Catalonia (Spain)
E-mail: guillem.aromi@qi.ub.es
Homepage: https://www.gmmf-ub.com

Supporting information for this article is given via a link at the end of the document.

In this work, CoO and CoO(OH) NPs have been obtained by decomposition in several organic solvents of the molecular Co^{II}/Co^{III} complex $[Co_8Na_4(L)_4(OH)_2(CO_3)_2(py)_{10}](BF_4)_2$ (**1**; py = Pyridine; L = 2,6-bis-(3-oxo-3-(2-hydroxyphenyl)-propionyl)-pyridine)[12] that are able to electrochemically form H_2 from water at pH 14. The NPs have been deposited onto the surface of a glassy carbon (GC) electrode after applying a potential of -1.86 V *vs.* NHE during 1 h in different solvents, and characterized by SEM, EDX, XPS and electrochemical techniques. The electrocatalytic properties of the as-deposited NPs and those of a new $Co(OH)_2$ phase generated under catalytic conditions have been analysed using the protocol for catalysts benchmarking recently reported by Jaramillo *et al.*[13] The implications of these results in the context of the current research in catalytic HER by Co-derived NPs are also discussed.

Results

Electrodeposition and characterization of Co-derived NPs

Two years ago, Aromí *et al.* described that the heptadentate ligand 2,6-bis-(3-oxo-3-(2-hydroxyphenyl)-propionyl)-pyridine (H_4L) reacts with Co(II) salts in strong basic conditions, yielding in the presence of atmospheric CO_2 the mixed Co^{II}/Co^{III} complex $[Co_8Na_4(L)_4(OH)_2(CO_3)_2(py)_{10}](BF_4)_2$ (**1**; py=pyridine) containing two trapped carbonate anions in very close proximity.[12] Given its unprecedented coordination features and the presence of 4 Co(II) and 4 Co(III) ions, we decided to study the potential applications of this complex in redox catalysis, specifically for the possible oxidative coupling of both trapped anions into a chemically interesting product. However, when studying its electrochemical features in acetonitrile (MeCN), two irreversible waves at -0.85 V and -1.50 V *vs.* NHE (-1.48 V and -2.13 V *vs.* Fc^+/Fc) and an irreversible oxidative wave near 0.35 V *vs.* NHE (-0.28 V *vs.* Fc^+/Fc) appeared, with a concomitant increase in their intensity upon performing several cyclic voltammetry (CV) cycles (Figure S1). This behaviour indicated that an irreversible chemical transformation of the electroactive species was taking place together with an increase of its available concentration at the electrode surface. This phenomenon could be related to an electrodeposition process on the surface of the GC electrode used for the measurements following the decomposition of **1** into bulk, nanoparticulated or layered Co-based materials. In fact, according to the literature, Co-based NPs able to electrochemically reduce water have already been reported to deposit at the electrode surface at modest cathodic potentials starting from a molecular Co(III) complex.[3a] Thus, we decided to test the possible deposition of Co-based NPs active in HER catalysis after an electrolysis of our system at more negative potentials than those of the first and second irreversible waves, *i.e.*, at -1.16 V and -1.86 V *vs.* NHE, respectively. The optimum electrolysis time resulted to be 1 h, since no significant changes in the size of the NPs nor their electrocatalytic activity (see below) were detected at higher electrolysis times. The SEM micrographs of the surface of the GC electrodes obtained are shown in Figures S2 and S3, respectively. The presence of NPs containing heavy nuclei is clear from the back-scattered electron SEM micrographs (bright spots) in both cases, with average diameters of 65.5 ± 18.2 and 52.5 ± 15.7 nm after the treatment at -1.16 V and -1.86 V, respectively *vs.* NHE. Furthermore, the elemental analysis by EDX of the SEM data (Figure S4) indicated the presence of Co in both samples, thus confirming the formation of Co-based NPs under these conditions. Additionally, the formation of Co-derived NPs can be deduced from the gradual loss of colour intensity of the MeCN solution of **1** during its electrolysis at -1.86 V *vs.* NHE and the appearance of dispersed colloidal particles after 16 h (Figure S5). The depletion of the original complex from the solution is confirmed by the complete disappearance of the characteristic absorbance band at 218 nm of **1** after 16 h (Figure S6).

Since the NPs obtained at -1.86 V *vs.* NHE show smaller size and higher uniformity (lower standard deviation of the average diameter) compared to those formed at -1.16 V, we decided to focus our attention on the former conditions to carry out our morphological and catalytic studies. It seems reasonable to expect higher catalytic activities with smaller NPs and thus with larger surface areas. Thus, an analogous procedure at -1.86 V *vs.* NHE was carried out in the presence of other solvents in which **1** is also soluble, namely dichloromethane (DCM) and methanol (MeOH). The SEM analyses showed the formation of smaller Co-derived NPs now, with average diameters of 37.5 ± 10.1 and 32.0 ± 9.3 nm for DCM and MeOH, respectively (Figures S7 and S8). Again, the presence of the element Co in the samples was confirmed by EDX (Figure S9). Furthermore, the ability of the octanuclear clustered complex **1** to transform into small and isolated NPs is demonstrated when analysing the results obtained under analogous conditions using $CoCl_2$ salt as Co precursor (Figure S10), now producing Co-derived NP aggregates of 0.28-0.45 μm in size with significant size dispersion.

In order to characterize the chemical composition of the as deposited-Co-derived NPs in MeCN, DCM and MeOH, XPS analyses were carried out (Figure 1 and Figure S11). The Co 2p XPS spectrum of the sample obtained in MeCN shows two main peaks at 780 and 796 eV accompanied by two broad satellite peaks at higher energies (786 and 802 eV), while for the samples obtained in DCM and MeOH the spectra are identical, basically showing only two main components at *ca.* 780.5 and 796 eV (Figure 1). The latter correspond to the Co $2p_{3/2}$ and Co $2p_{1/2}$ components, respectively,[14] while the satellite peaks indicate the presence of unpaired electrons in the sample, *i.e.*, of Co^{II} (d^7) atoms.[15] The O 1s XPS spectra, show a single band at 530.5 eV for the MeCN sample, which is shifted towards 531.4 eV for the DCM and MeOH cases (Figure S11a). This shift towards higher energies is due to the presence of hydroxyl groups on

the Co surface.[2,7,14,16] Thus, when taking all XPS data in consideration, it is clear that in MeCN we obtain CoO NPs. This is supported by the similarity of our Co 2p XPS spectrum with those of CoO previously reported[15] and by the presence of a band at *ca.* 530 eV for the O 1s XPS spectrum, as reported elsewhere.[7,14] In sharp contrast, in DCM and MeOH mixed oxy-hydroxide Co^{III} (d^6) NPs are obtained (CoO(OH) NPs) based on the almost complete absence of Co 2p satellite bands and the 780.5 eV value for the Co $2p_{3/2}$ transtion[17] as well as on the high energy shift of the O 1s band. The presence of CoO(OH) in the sample formed in DCM could be due to hydration processes provoked by air exposure prior to the XPS measurements. Regarding N and C XPS signals (Figure S11b-c), the N 1s band found *ca.* 399 eV for all samples is typical of Co-N bonds or N-pyridyls,[4a-b,6] which originate from ligand L in precursor **1** during its electrodecomposition (a comparison of the N atomic percentage measured by XPS indicates that the amount of N of the samples is comprised between 8 and 15 % and thus is not negligible compared to the 0.7 % atomic percentage of the blank), and the C 1s band at *ca.* 284.2 eV is due to the GC electrode.[18] From now on in this work and for the sake of brevity, the three sets of NPs formed after 1h-electrolysis at -1.86 V *vs.* NHE will be named as CoO-MeCN, CoO(OH)-MeOH and CoO(OH)-DCM.

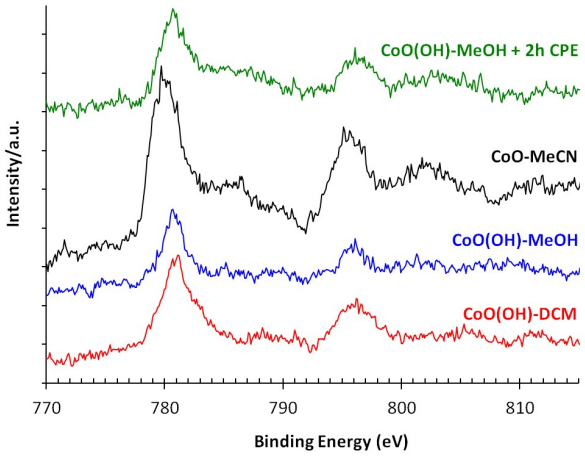

Figure 1. Co 2p XPS spectra for the Co-based NPs obtained from **1** in MeCN (black), DCM (red) and MeOH (blue) after a 1h-electrolysis at -1.86 V *vs.* NHE and from **1** in MeOH after a 1h-electrolysis at -1.86 V *vs.* NHE plus a 2h-CPE at 10 $mA \cdot cm^{-2}$ (green). Energies have been calibrated according to the C 1s band of graphite at 284.2 eV.

Electrocatalytic performance

The Co-derived NPs deposited on the surface of a rotating disk electrode (RDE) obtained in the three different solvents were characterized by rotating disk voltammetry (RDV) at pH 14 (Figure 2), where an intense irreversible catalytic current with onset potential at *ca.* -1.11, -1.15 and -1.20 V *vs.* NHE appears for CoO-MeCN, CoO(OH)-MeOH and CoO(OH)-DCM, respectively, with associated current densities of 1.27, 0.76 and 0.26 mA/cm^2. According to H_2-sensitive Clark electrode measurements, this process corresponds to the reduction of protons to generate H_2 with a faradaic efficiency between 96% and 98% for all cases (Figure S12). From the experimental onset potential of the catalytic waves compared to the thermodynamic reduction potential $E(H^+/H_2)$ at pH 14 (-0.828 V *vs.* NHE), the MeCN, MeOH and DCM samples show an onset overpotential of -276 mV, -321 mV and -348 mV, respectively.

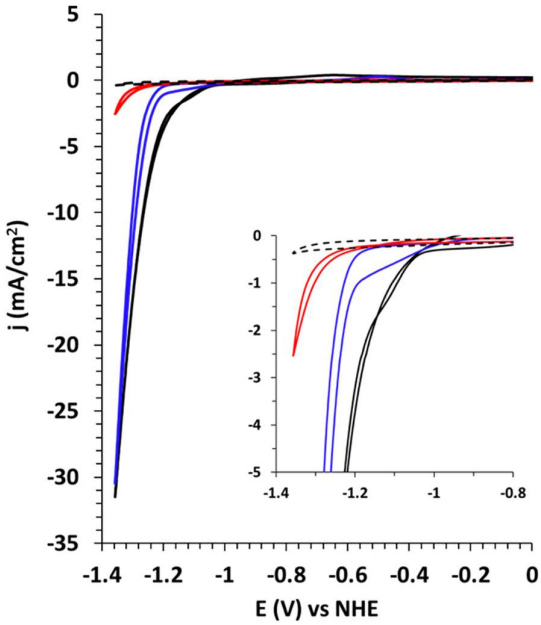

Figure 2. Representative rotating disk voltammograms of CoO(OH)-DCM (red), CoO(OH)-MeOH (blue) and CoO-MeCN (black). The non-functionalized RDE electrode (blank) is shown as a black dashed line. Conditions: N_2-Saturated 1 M NaOH solution, 0.01 V/s scan rate and 1600 rpm. Inset: zoomed view of the onset potential region.

A thorough electrochemical analysis of the behaviour of the Co-based NPs has been performed following the procedures described by Jaramillo *et al.*[13] Thus, the electrochemically active surface area (ECSA) of each modified RDE with Co-based NPs was estimated from its electrochemical double-layer capacitance (C_{dl}) by measuring the non-Faradaic capacitive current associated with double-layer charging (Figure S13). The roughness factor (RF) is calculated by dividing the estimated ECSA by the geometric area of the electrode. Furthermore, 30s-controlled current step-chronopotentiometry and chronoamperometry (Fig. S14) and 2h-controlled current electrolysis (Figure 3a and Fig. S15) measurements have allowed us to determine the overpotential at a constant current density of 10 $mA \cdot cm^{-2}$ (η). This is a widely accepted benchmarking parameter for the catalytic activity of heterogeneous catalysts which

corresponds to the approximate current density expected for a 10% efficient solar-to-fuel conversion photoelectrochemical cell under 1 sun illumination[19] (Figure S14). The NPs with lower η are CoO-MeCN (-435 mV), followed by CoO(OH)-MeOH (-465 mV) and finally by CoO(OH)-DCM (-504 mV). Interestingly, when the CoO-MeCN and CoO(OH)-DCM NPs are submitted to a 2h-controlled current electrolysis at a constant current density of 10 mA·cm^{-2} (Figure S15), the η steadily increases, particularly for CoO-MeCN, denoting the relative instability of both systems under HER conditions. Effectively, XPS (Fig S16) and SEM analyses (Fig. S17 and S18) show the lack of stability of both CoO-MeCN and CoO(OH)-DCM NPs after a 2h-controlled current electrolysis. For the former case, no Co-derived NPs are detected on the surface of the GC electrode, and for the latter the CoO(OH) composition of the NPs is maintained, although their concentration clearly decreases (less intense Co 2p signal and decrease of the Co atomic concentration from 1.61 % to 0.64 % according to XPS measurements, Fig. S16) while at the same time the average diameter increases from 37.5 nm (Figure S7) to 77.7 nm (Figure S18).

In contrast, as shown in Figure 3a, the η of CoO(OH)-MeOH NPs clearly decreases over time. The superior activity of the resulting nanomaterial after electrolysis is also appreciated when comparing its RDV with that of the original CoO(OH) NPs in the same conditions (Figure 3b). A detailed electrocatalytic analysis of this "activated" system can be found in Figures S19-S21 of the Supplementary Material. The results corroborate its higher performance, with a decrease in η by 213 mV and a significant increase in the specific current density (j_s) at an overpotential of -480 mV, which is more than triplicated, from 174 to 596 mA·cm^{-2}.

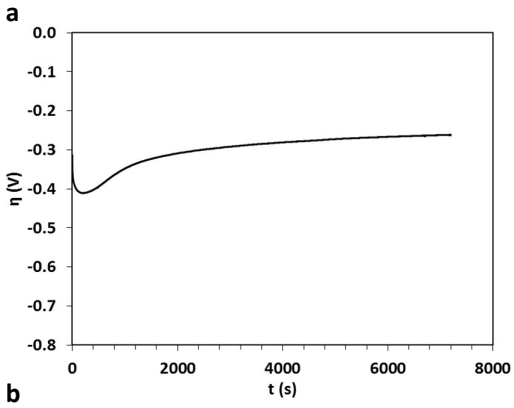

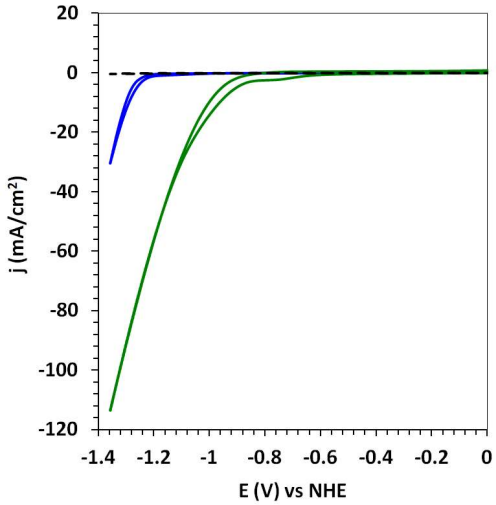

Figure 3. a) 2h-controlled current electrolysis in MeOH at 10 mA·cm^{-2} of CoO(OH)-MeOH; b) representative rotating disk voltammograms of CoO(OH)-MeOH at t=0 (blue) and after a 2h-controlled current electrolysis at 10 mA·cm^{-2} (green). The non-functionalized RDE electrode (blank) is shown as a dashed line. Conditions: N_2-Saturated 1 M NaOH solution, 0.01 V/s scan rate and 1600 rpm.

In order to better understand the nature of this "activated" system, the 2h-electrolized cathode was characterized by SEM (Fig. S22 and S23) and XPS (Figure 1 and Figure S11). SEM images show an average diameter of 39.9 ± 16.4 nm, very close to the precursor CoO(OH) NPs before the activation (Figure S8).

Comparison of the Co 2p XPS spectra of the CoO(OH)-MeOH sample and its 2h-electrolyzed derivative shows the appearance of two satellite bands for the latter (Figure 1) and the presence of an O 1s XPS band at 531.2 eV in both samples (Figure S11a). Thus, a reduction of the Co^{III} atoms to Co^{II} is taking place without losing hydroxyl groups. Therefore, we propose the formation of $Co(OH)_2$ NPs after the 2h activation process in MeOH. Indeed, the positions of the Co 2p main peaks at 780.7 and 796.5 eV as well as the overall shape of the spectrum are coincident with previous data reported for $Co(OH)_2$.[8,11a,15,17] Curiously, the low intensity shoulder at *ca.* 287.5 eV of its C 1s XPS spectrum (Figure S11c) could be attributed to the presence of MeOH molecules coordinated onto the surface of the $Co(OH)_2$ NPs.[20]

Finally, the Tafel plots for all four Co-derived NPs and two blanks prepared in MeOH from $CoCl_2$ and $CoCl_2$ in the presence of H_4L are shown in Figure 4, in which it becomes clear the superior HER activity of the $Co(OH)_2$ NPs obtained after a 2h-CPE in MeOH (red line).

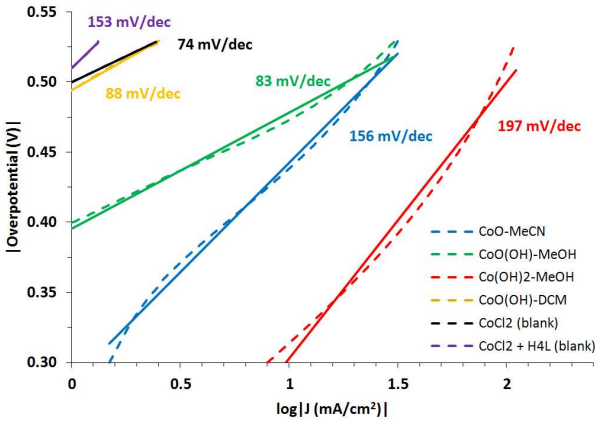

Figure 4. Tafel plots registered at pH 14 for the Co-based NPs synthesized in this work in different solvents and from $CoCl_2$ or $CoCl_2$ + H_4L in MeOH (blanks).

Discussion

A comparison of the physical and electrochemical properties of the Co-derived NPs formed from **1** in this work with those of the respective blanks prepared from $CoCl_2$ is shown in Table 1. In all cases, the NPs obtained in the blanks (entries 5-8) are one order of magnitude larger and less uniformly sized than their respective NPs formed from **1** (entries 1-3), showing the relevant role of the molecular precursor for its proper reduction into small Co-derived NPs. This result highlights the already reported role of metal complexes in allowing better control over *in-situ* electrodeposition processes than simple salts.[10b] Thus, the initial η ($\eta_{t=0}$) and the η value after 2h-electrolysis ($\eta_{t=2}$) are normally higher than the respective values for the NPs obtained from **1** (entries 1 *vs.* 5, 2 *vs.* 6 and 3 *vs.* 7) while the j_s values are between 1 and 3 orders of magnitude lower. Also, the presence of uncoordinated H_4L ligand in the $CoCl_2$ blank prepared in MeOH does not significantly alter the performance of the obtained NPs compared to the blank prepared in its absence (entries 7 and 8), thus pointing to the importance of starting from a precursor containing the ligand within its molecular scaffold.

Table 1. Physical and electrochemical properties of the Co-derived NPs synthesized in this work onto the surface of a RDE electrode.

Entry	Co Precursor	Solvent	NP[a]	diameter (nm)[b]	ECSA[c]	RF[c]	Onset η (mV)[d]	$\eta_{t=0}$ (mV)[e]	$\eta_{t=2}$ (mV)[f]	j_s @ η=-480 mV (mA·cm^{-2})[g]	ε[h]
1	**1**	MeCN	CoO	52.5 ± 15.7	0.14 ± 0.02	1.14 ± 0.19	-276 ± 47	-435 ± 29	-669 ± 37	225 ± 30	96%
2	**1**	DCM	CoO(OH)	37.5 ± 10.1	0.08 ± 0.01	0.65 ± 0.11	-348 ± 28	-504 ± 20	-595 ± 12	20 ± 10	98%
3	**1**	MeOH	CoO(OH)	32.0 ± 9.3	0.15 ± 0.02	1.24 ± 0.18	-321 ± 78	-465 ± 98	-252 ± 16	174 ± 124	98%
4	CoO(OH)	MeOH	$Co(OH)_2$[i]	39.9 ± 16.4	0.15 ± 0.02	1.24 ± 0.18	-140 ± 74	-246 ± 20	n.d.	596 ± 216	98%
5	$CoCl_2$	MeCN	n.d[j]	448 ± 146	0.14 ± 0.04	1.21 ± 0.06	-367 ± 80	-461 ± 97	n.d.	0.46 ± 0.28	n.d.
6	$CoCl_2$	DCM	n.d.	325 ± 280	0.08 ± 0.01	0.64 ± 0.09	-390 ± 60	-475 ± 70	n.d.	0.56 ± 0.31	n.d.
7	$CoCl_2$	MeOH	n.d.	283 ± 175	0.13 ± 0.02	1.07 ± 0.19	-398 ± 15	-515 ± 88	-679 ± 70	15 ± 14	n.d.
8	$CoCl_2$ + H_4L	MeOH	n.d.	n.d.	0.16 ± 0.02	1.24 ± 0.20	-406 ± 45	-544 ± 30	-572 ± 20	11 ± 8	n.d.

[a] Formed during 1h-electrolysis at -1.86 V *vs.* NHE at 1600 rpm and determined by XPS analyses. [b] Determined by SEM analyses. [c] Electrochemically-active surface area (ECSA) and roughness factor (RF) determined according to Jaramillo *et al.*[13] The double-layer capacitance of the systems has been calculated as the average of the absolute value of the slopes of their linear fits to the data shown in Figures S13 and S19. [d] Onset overpotential of the electrocatytic wave estimated from RDV experiments. [e] Overpotential required for reaching a 10 mA·cm^{-2} current density. The values have been estimated from the 30 s step-chronopotentiometry and chronopotentiometry experiments. [f] Overpotential required for reaching 10 mA·cm^{-2} current density after a 2h-controlled current electrolysis experiment. [g] Specific current density (j_s) obtained by dividing the experimental current density (j, in mA·cm^{-2}) by the ECSA at an overpotential of -480 mV. [h] ε = Faradaic efficiency. [i] The precursor are the CoO(OH) NPs obtained in MeOH after 1h-electrolysis of **1** at -1.86 V *vs.* NHE, which are then submitted to a 2h-CPE experiment at 10 mA·cm^{-2}. [j] n.d. = not determined.

The ECSA and RF values of our Co-based NPs are similar, assuming the one order of magnitude inherent accuracy of the RF measurements, while they are significantly lower -around three orders of magnitude- than those of Co electrodes previously benchmarked.[13] These results are consistent with the fact that in our case low concentrations of **1** are used for the NP electrodeposition

(0.25 mM) compared to the much higher concentrations used in the literature (around 100 mM).[13] The low ECSA values combined with the high catalytic currents measured translate into particularly high specific current densities (j_s) in the HER when measured at an overpotential of -480 mV (entries 1-4, Table 1).

On the other hand, the CoO-MeCN and CoO(OH)-DCM NPs suffer from an increase in η over time (entries 1 and 2), specially in the former case. This decrease in the HER activity is more pronounced than that previously reported for the best metallic cathodes by Jaramillo *et al.*[13] Furthermore, the XPS and SEM measurements performed after a 2h-CPE (Figs. S16-S18) have shown the instability of these nanoparticulated systems, probably due to the inability of MeCN and DCM to form stabilizing hydrogen bonds with the NPs (see below). However, despite this drawback, our Faradaic efficiencies are comprised in the 96-98% range, which stand out among the normal values found for some of the best metal-based HER catalysts reported so far at pH 14.[13]

Contrastingly, CoO(OH)-MeOH NPs undergo a dramatic decrease in η over time while being converted into $Co(OH)_2$ NPs (entries 3 and 4), reaching a $\eta_{t=2}$ value as low as *ca.* -250 mV at pH 14. This overpotential is lower than that of other published Co-based NP systems under analogous conditions. Thus, Co NPs encapsulated in N-rich CNTs have shown an η of -375 mV at pH 14,[3b] whereas Co/CoO[5] and Co NPs[4a] immobilized on N-doped and Co-N-doped C feature η values of -395 and -314 mV, respectively, at pH 13. Also, a similar η of -250 mV has been measured at pH 14 for Co NPs on N,S-doped C[6] and for trimetallic CoNiFe NPs.[13] Additional data on additional recently published Co-derived nanosystems applied in electrochemical HER catalysis can be found in Table S1.

Concerning the CoO(OH)-DCM NPs, it is difficult to rationalize why, having very similar size and RF values as those of CoO(OH)-MeOH (entries 2 and 3), they clearly possess lower HER catalytic activity and stability (*i.e.*, higher η -specially over time- and one order lower j_s value, and even higher $\eta_{t=0}$ than its $CoCl_2$ blank counterpart). This may be due in part to slower mass transport of H^+ into the NPs in the case of DCM, as suggested by Jaramillo *et al.* during the catalytic performance of metallic nanoporous films compared to non-nanoporous films made from the same metal.[13] Thus, the CoO(OH) NPs obtained in DCM may have a different structure than those synthesized in MeOH, probably because of the non-coordinating and non-hydrogen bonding ability of DCM, which may lead to less stable NPs. In fact, previous studies with metallic NPs have demonstrated their morphology dependence with the nature/polarity of the solvent employed for their synthesis.[21] Furthermore, it is likely that the hydrogen binding abilities of MeOH -completely absent in DCM and MeCN- may play a key role in the stabilization of CoO(OH) NPs and their further conversion into the more active $Co(OH)_2$ NPs during the 2h-CPE. Contrastingly, the non-hydrogen binding abilities of both DCM and MeCN may be one of the reasons for the progressive deactivation of the CoO(OH)-DCM and CoO-MeCN NPs along time. Nonetheless, the amount of N and C coming from the ligand initially present in **1** or fragments of it within all Co-derived NPs (see N 1s and C 1s XPS data of Figure S11b-c of the Supplementary Material) should not be ignored, since these elements may not only contribute to the formation of small and highly dispersed NPs but could also provide a stabilizing effect to the NPs during catalysis. However, an exact determination of the amount of C and N originating from **1** is not possible given the use of GC electrodes as supports and the presence of N in the supporting electrolyte ($TBAPF_6$) and in MeCN.

Finally, from the analysis of the Tafel plots (Figure 4) it also becomes obvious that the three more active systems (the ones on the right hand side of the graph) are those obtained from **1** in MeCN and MeOH (in fact, the activity of CoO(OH)-DCM is very close to that of the $CoCl_2$ blank obtained in MeOH). The slopes for CoO-MeCN, CoO(OH)-MeOH and $Co(OH)_2$ are close or above 100 mV/dec. Therefore, consistent with the literature,[22] the rate determining step (rds) for the HER reaction in our three most active systems must be the Volmer step, i.e., the electrochemical H adsorption onto the NP surface. On the other hand, the crossing of the CoO-MeCN (blue line) and the CoO(OH)-MeOH (green line) curves confirms that the former is more active (higher *j*) at an overpotential lower than *ca.* -520 mV, but that at overpotentials more negative than -520 mV the latter performs better in HER.

Conclusions

In this work, we have demonstrated that the molecular Co^{II}/Co^{III} complex **1** generates electrodeposited ~50 nm CoO or ~35 nm CoO(OH) NPs depending on the solvent employed (MeCN for the former, MeOH or DCM for the latter) from its decomposition at -1.86 V *vs.* NHE. The resulting cathodes, possessing low and comparable ECSA and RF values, catalyze the electrochemical reduction of water at pH 14 with distinctive specific activities (j_s) under the application of a -480 mV bias. The most active system at t=0 h is CoO-MeCN ($\eta_{t=0}$=-435 mV, j_s=225 mA·cm^{-2} at an overpotential of -480 mV). However, the CoO(OH)-MeOH NPs, with an initial catalytic activity very close to those of CoO-MeCN, become significantly more active after a 2h constant polarization process at 10 mA·cm^{-2} ($\eta_{t=2}$=-250 mV, j_s=596 mA·cm^{-2} at an overpotential of -480 mV). These activated NPs correspond to $Co(OH)_2$ according to XPS analysis, which show better HER performance than many Co-based NP systems published elsewhere under analogous conditions. Contrastingly, the HER activity steadily decreases for CoO-MeCN and CoO(OH)-DCM during a 2h-chronopotentiometry experiment at 10 mA·cm^{-2}. This decrease in activity is proposed to be mainly related to the inability of these solvents to form stabilizing hydrogen bonds with the NPs, in contrast to MeOH. Finally, the observed increase in H_2 evolution activity with increasing presence of hydroxyl groups in the series CoO(OH)<$Co(OH)_2$ observed during the 2h-

chronopotentiometry in MeOH is in agreement with previous results in the literature.[8] However, further structural studies of the surfaces of both CoO(OH) systems obtained in DCM and MeOH are under way to fully understand their markedly different catalytic performance.

Experimental Section

All reagents used in the present work were obtained from Sigma Aldrich in reagent grade and were used without further purification. Reagent grade organic solvents were obtained from Scharlab and Panreac. Anhydrous $CoCl_2$ was supplied by Sigma Aldrich. NaOH was obtained from Panreac (99%), and milliQ quality grade water was employed. $[Co_8Na_4(L)_4(OH)_2(CO_3)_2(py)_{10}](BF_4)_2$ (**1**) was prepared as previously reported.[12]

UV-Vis spectroscopy was performed on a HP8453 spectrometer using 1 cm quartz cells. Scanning Electron Microscopy (SEM) and Energy-dispersive X-Ray Spectroscopy (EDX) analyses were performed using a JEOL JSM 6700F electron microscope working at 10 kV.

X-ray photoelectron spectroscopy (XPS) experiments were performed with a SPECS EA10P hemispherical analyser using a non-monocromated X-ray source (Al Kα line of 1486.6 eV and 300W). The direction of the X-ray source with respect to the sample was 90º and ultrahigh vacuum was maintained during the measurements, obtaining a residual pressure of 10^{-8} Pa. GC electrodes analysed by SEM and XPS were functionalized for 1h by applying a constant potential (-1.86 V or -1.16 V *vs.* NHE) to a solution of **1** (0.6 mg, 2 µmol) in the different solvents assayed. Afterwards, the GC surface was washed with distilled H_2O, MeCN and acetone. Then, a small section of the electrode was cut on a Mintom rotating saw (Struers) equipped with a metal cut-off wheel, washed again with distilled H_2O, acetone and Et_2O and dried over vacuum for 2h.

Electrochemical measurements were carried out on a Bio Logic Science Instrument SP-150 potentiostat and CHI660D potentiostat using a three-electrode cell. A glassy carbon (GC, 3 mm internal diameter) or a rotating disk electrode (RDE, 4 mm GC disk diameter) were employed as working electrodes, while a platinum wire was used as counter electrode and $Hg/HgSO_4$ or SCE were used as the reference electrodes. The solvents used for functionalization of the electrode (acetonitrile, methanol or dichloromethane) were prepared containing the necessary amount of n-Bu_4NPF_6 ($TBAPF_6$) as supporting electrolyte to yield a 0.1 M ionic strength. Electrodeposition of Co NPs was carried out in a 10 mL three electrode cell using RDE as working electrode, platinum as counter electrode and $Hg/HgSO_4$ as reference electrode. Before each functionalization, the RDE electrode was polished with 1 and 0.05 micron alumina suspension in distilled water, sonicated for 5 min in H_2O and washed with distilled water and acetone before each measurement. 1 mg (0.3 µmol) of **1** was sonicated in the 10 mL three electrode cell until complete solution in 3 mL of the corresponding organic solvent (MeCN, DCM or MeOH) containing 0.1 M of electrolyte ($TBAPF_6$). Subsequently, a constant potential of -1.86 V or -1.16 V *vs.* NHE was applied to the solution for 1 hour. Finally, the functionalized RDE electrode was washed with distilled H_2O, MeCN and acetone and dried over vacuum for 30 minutes before electrochemical measurements.

For the electrochemical characterization and catalytic experiments in HER, the cell was purged for 30 minutes with N_2 and was continuously bubbled during the measurements. The resistance of the cell (typically R_u ~ 13 Ω) was compensated at 85%. In the case of electrochemical capacitance measurements, linear sweep voltammetry (LSV) was performed in a potential window where there is a non-Faradaic current response as determined from cyclic voltammetry. This range is typically 0.1 V centred on the Open-circuit potential (OCP) for each electrode. The measurements were carried out by sweeping the potential across the selected potential range at 8 different scan rates (0.005, 0.01, 0.025, 0.05, 0.1, 0.2, 0.4, 0.8 V/s). The working electrode was held at the starting potential before beginning the next LSV experiment.

For Faradaic efficiency measurements, H_2 was quantified using a Unisense H_2-probe controlled by a Unisense Microprocessor Multimeter. Measurements were carried out in a U-compartment cell containing a functionalized GC electrode (3 mm diameter), a reference electrode (Ag/AgCl) and the hydrogen probe in the first compartment and a counter electrode in the second compartment, both separated by a frit and filled with 15 mL of NaOH solution (pH 14). For H_2 measurements, the solution was degassed with a N_2 flow for 30 minutes under vigorous stirring. The baseline was recorded for 20 minutes and a constant potential of -1.86 V *vs.* NHE was held at the working electrode containing Co NPs for 30 min. The increase in pressure of H_2 was monitored during this time, and from this the total amount of H_2 gas formed was determined. Finally, Faradaic efficiency was calculated by dividing the total amount of H_2 produced during the experiment by the theoretical amount calculated from the total charge passed in the bulk-electrolysis experiment.

Acknowledgements

Support from MINECO/FEDER (CTQ2015-64261-R and CTQ2016-80058-R) is gratefully acknowledged. M. G.-S. is grateful for the award of a PIF doctoral grant from UAB. J. G.-A. acknowledges the Serra Húnter Program. G. A., D. A. and V. V. thank the ERC for contracts under ERC Starting Grant StG-2010-258060 and the Generalitat de Catalunya for the prize ICREA Academia 2008 and 2013. We also thank the Servei de Microscopia Electrònica, Universitat Autònoma de Barcelona, for allocating instrument time.

Keywords: CoO • CoO(OH) • $Co(OH)_2$ • H_2 evolution

[1] a) Z. Han, R. Eisenberg, *Acc. Chem. Res.* **2014**, *47*, 2537-2544; b) M. Wang, K. Han, S. Zhang, L. Sun, *Coord. Chem. Rev.* **2015**, *287*, 1-14; c) Y. Xu, B. Zhang, *Cat. Sci. & Tech.* **2015**, *5*, 3084-3096; d) N. Jiang, B. You, M. Sheng, Y. Sun, *Angew., Chem. Int. Ed.* **2015**, *54*, 6251-6254; e) B. You, N. Jiang, M. Sheng, M. W. Bhushan, Y. Sun, *ACS Catal.* **2016**, *6*, 714-721; f) B. You, X. Liu, X. Liu, Y. Sun, *ACS Catal.* **2017**, *7*, 4564-4570; g) B. You, Y. Sun, *Adv. Energy Mater.* **2016**, *6*, 1502333.

[2] S. Fukuzumi, Y. Yamada, *J. Mater. Chem.* **2012**, *22*, 24284-24296.

[3] a) E. Anxolabéhère-Mallart, C. Costentin, M. Fournier, S. Nowak, M. Robert, J.-M. Savéant, *J. Am. Chem. Soc.* **2012**, *134*, 6104-6107; b) X. Zou, X. Huang, A. Goswami, R. Silva, B. R. Sathe, E. Mikmekov, T. Asefa, *Angew. Chem., Int. Ed.* **2014**, *53*, 4372-4376; c) E. Zhang, Y. Xie, S. Ci, J. Jia, P. Cai, L. Yia, Z. Wen, *J. Mat. Chem. A* **2016**, *4*, 17288-17298.

[4] a) Y. Wang, Y. Nie, W. Ding, S. G. Chen, K. Xiong, X. Q. Qi, Y. Zhang, J. Wang, Z. D. Wei, *ChemComm.* **2015**, *51*, 8942-8945; b) H. Su, H.-H. Wang, B. Zhang ,K.-X. Wang, X.-H. Lin, J.-S. Chenn, *Nano Energy* **2016**, *22*, 79-86.

[5] X. Zhang, R. Liu, Y. Zang, G. Liu, G. Wang, Y. Zhang, H. Zhang, H. Zhao, *ChemComm.* **2016**, *52*, 5946-5949.

[6] W. Deng, H. Jiang, C. Chen, L. Yang, Y. Zhang, S. Peng, S. Wang, Y. Tan, M. Ma, Q. Xie, *ACS Appl. Mater. Interfaces* **2016**, *8*, 13341-13347.

[7] X. Liu, C. Dong, W. Dong, X. Wang, X. Yuan, F. Huang, *RSC Adv.* **2016**, *6*, 38515-38520.

[8] Z. Li, Y. Wu, G. Lu, *Appl. Cat. B: Environm.* **2016**, *188*, 56-64.

[9] a) H. Dang, X. Dong, Y. Dong, H. Fan, Y. Qiu, *Mater. Lett.* **2015**, *138*, 56-59; b) H. Wender, R. V. Gonçalves, C. S. B. Dias, M. J. M. Zapata, L. F. Zagonel, E. C. Mendonça, S. R. Teixeira, F. Garcia, *Nanoscale* **2013**, *5*, 9310-9316.

[10] a) R. K. Hocking, R. Brimblecombe, L.-Y. Chang, A. Singh, M. H. Cheah, C. Glover, W. H. Casey, L. Spiccia, *Nat. Chem.* **2011**, *3*, 461-466; b) A. Singh, R. K. Hocking, S. L.-Y. Chang, B. M. George, M. Fehr, K. Lips, A. Schnegg, L. Spiccia, *Chem. Mater.* **2013**, *25*, 1098-1108.

[11] a) D. Hong, J. Jung, J. Park, Y. Yamada, T. Suenobu, Y.-M. Lee, W. Nam, S. Fukuzumi, *Energy Environ. Sci.* **2012**, *5*, 7606–7616; b) J. J. Stracke, R. G. Finke, *J. Am. Chem. Soc.* **2011**, *133*, 14872-14875.

[12] V. Velasco, D. Aguilà, L. A. Barrios, I. Borilovic, O. Roubeau, J. Ribas-Ariño, M. Fumanal, S. J. Teat, G. Aromí, *Chem. Sci.* **2015**, *6*, 123-131.

[13] C. C. L. McCrory, S. Jung, I. M. Ferrer, S. M. Chatman, J. C. Peters, T. F. Jaramillo, *J. Am. Chem. Soc.* **2015**, *137*, 4347–4357.

[14] A. Indra, P. W. Menezes, C. Das, C. Göbel, M. Tallarida, D. Schmeißer, M. Driess, *J. Mat. Chem. A* **2017**, *5*, 5171-5177.

[15] M. C. Biesinger, B. P. Payne, A. P. Grosvenor, L. W. M. Lau, A. R. Gerson, R. St. C. Smart, *Appl. Surf. Sci.* **2011**, *257*, 2717-2730.

[16] J. Fester, M. García-Melchor, A. S. Walton, M. Bajdich, Z. Li, L. Lammich, A. Vojvodic, J. V. Lauritsen, *Nat. Commun.* **2017**, *8: 14169*, 1-8.

[17] J. Yang, H. Lu, W. N. Martens, R. L. Frost, *J. Phys. Chem. C* **2010**, *114*, 111-119.

[18] a) L. J. Fang, X. L. Wang, Y. H. Li, P.F. Liu, Y. L. Wang, H. D. Zeng, H. G. Yang, *Appl. Catal B: Environ.* **2017**, *200*, 578-584; b) X. Yue, S. Yi, R. Wang, Z. Zhang, S. Qiu. *Nat. Sci. Reports* **2017**, *6:22268*, 1-8.

[19] M. G. Walter, E. L. Warren, J. R. McKone, S. W. Boettcher, Q. Mi, E. A. Santori, N. S. Lewis, *Chem. Rev.* **2010**, *110*, 6446-6473.

[20] A. K. Agegnehu, C.-J. Pan, J. Rick, J.-F. Lee, W.-N. Su, B.-J. Hwang, *J. Mater. Chem.* **2012**, *22*, 13849-13854.

[21] K. Pelzer, O. Vidoni, K. Philippot, B. Chaudret, V. Collière, *Adv. Funct. Mater.* **2003**, *13*, 118-126.

[22] Y. Zheng, Y. Jiao, M. Jaroniec, S. Z. Qiao. *Angew. Chem., Int. Ed.* **2015**, *54*, 52-65.